Clim Dyn (2007) 29:195–210
DOI 10.1007/s00382-007-0230-4

Changes in storm track and cyclone activity in three SRES ensemble experiments with the ECHAM5/MPI-OM1 GCM

J. G. Pinto · U. Ulbrich · G. C. Leckebusch · T. Spangehl · M. Reyers · S. Zacharias

Received: 8 June 2006 / Accepted: 16 January 2007 / Published online: 22 February 2007

Abstract Synoptic activity over the Northern Hemisphere is evaluated in ensembles of ECHAM5/MPI-OM1 simulations for recent climate conditions (20C) and for three climate scenarios (following SRES A1B, A2, B1). A close agreement is found between the simulations for present day climate and the respective results from reanalysis. Significant changes in the winter mid-tropospheric storm tracks are detected in all three scenario simulations. Ensemble mean climate signals are rather similar, with particularly large activity increases downstream of the Atlantic storm track over Western Europe. The magnitude of this signal is largely dependent on the imposed change in forcing. However, differences between individual ensemble members may be large. With respect to the surface cyclones, the scenario runs produce a reduction in cyclonic track density over the mid-latitudes, even in the areas with increasing mid-tropospheric activity. The largest decrease in track densities occurs at sub-tropical latitudes, e.g., over the Mediterranean Basin. An increase of cyclone intensities is detected for limited areas (e.g., near Great Britain and Aleutian Isles) for the A1B and A2 experiments. The changes in synoptic activity are associated with alterations of the Northern Hemisphere circulation and background conditions (blocking frequencies, jet stream). The North Atlantic Oscillation index also shows increased values with enhanced forcing. With respect to the effects of changing synoptic activity, the regional change in cyclone intensities is accompanied by alterations of the extreme surface winds, with increasing values over Great Britain, North and Baltic Seas, as well as the areas with vanishing sea ice, and decreases over much of the subtropics.

J. G. Pinto (✉) · M. Reyers · S. Zacharias
Institut für Geophysik und Meteorologie,
Universität zu Köln, Kerpener Str. 13,
50923 Cologne, Germany
e-mail: jpinto@meteo.uni-koeln.de

M. Reyers
e-mail: mreyers@meteo.uni-koeln.de

S. Zacharias
e-mail: szach@meteo.uni-koeln.de

U. Ulbrich · G. C. Leckebusch · T. Spangehl
Institut für Meteorologie, Freie Universität Berlin,
Carl-Heinrich-Becker-Weg 6-10,
12165 Berlin, Germany
e-mail: ulbrich@met.fu-berlin.de

G. C. Leckebusch
e-mail: gcl@met.fu-berlin.de

T. Spangehl
e-mail: spangehl@met.fu-berlin.de

1 Introduction

Weather phenomena in the extra-tropical latitudes are often associated with migratory cyclones travelling in the belt of prevailing westerly winds (Charney 1947). The westerlies are generally baroclinic unstable all through the year, and the development of such cyclonic eddies is a fundamental feature of the general circulation of the atmosphere (Bengtsson 1991). These synoptic scale disturbances are characterised by periods ranging from a few days to about a week (Wallace et al. 1988). A common approach to quantify the synoptic scale wave activity is the calculation of the

bandpass-filtered variance in the 500 hPa height field, and the regions of strongest baroclinic wave activity are referred to as storm tracks (Eulerian approach, e.g., Blackmon 1976; Blackmon et al. 1977; Wallace et al. 1988; Hoskins and Valdes 1990). An alternative perspective is the analysis of cyclone lifecycles and their statistics from genesis to decay (Lagrangian approach, e.g., Lambert 1988; Murray and Simmonds 1991; Hodges 1995, 1999). Both views contribute to a better assessment of barocline waves and their importance not only in the heat and momentum budget of the atmosphere (Peixoto and Oort 1992), but also in regional weather, notably winds, precipitation and major hazards associated with the most intense storms (Bengtsson 1991).

Both perspectives may be used to quantify baroclinic wave activity in reanalysis data (e.g., Hoskins and Valdes 1990; Hoskins and Hodges 2002), and in General Circulation Models (GCMs) (e.g., König et al. 1993; Knippertz et al. 2000). GCM simulations are able to reproduce well the extra-tropical storm tracks if resolution is sufficient (e.g., Bengtsson 1991). This is particularly pertinent when concerning the projected changes in Greenhouse Gas (GHG) forcing in the next 100 years (e.g., Cubasch et al. 2001), as changes in location and intensity of the storm tracks may severely affect the climate over the Northern Hemisphere (NH) mid-latitudes.

There have been contradictory reports on significant changes of storm activity in the second half of the twentieth century based on reanalysis and observational data: while some authors reported increased activity (e.g., Geng and Sugi 2001; McCabe et al. 2001; Paciorek et al. 2002), others mention that storminess has been remarkably stationary in the last 200 years, with little fluctuations on time scales of more than one or two decades (e.g., WASA group 1998; Barring and von Storch 2004). Moreover, Bengtsson et al. (2004) reported that these trends may not be reliable because of inhomogeneities in the reanalysis data series, as an incremental increase is found in many variables (e.g., kinetic energy) in the extra-tropics around 1978/1979, coinciding with the introduction of the global observing system.

In recent years, ensemble simulations approaches in climate change research have become frequent, as they allow to address modelling uncertainties and therefore provide more reliable results. Efforts like the current Intergovernmental Panel on Climate Change (IPCC) Fourth Assessment Report (AR4) have encouraged the scientific community to further explore this path. With this aim, we will consider an ensemble of simulations by the coupled ECHAM5/MPI-OM1 (European Centre Hamburg Version 5/Max Planck Institute—Ocean Model Version 1; cf. Roeckner et al. 2003) GCM run under three different scenarios, based on the Special Report on Emission Scenarios (SRES, cf. Nakićenović et al. 2000). As pointed out by Räisänen (2001), it is essential to select not only a single best estimate of future climate but also to try to estimate the ''probability of distribution'' of possible outcomes. Therefore, the three member ensemble is used in order to sample the uncertainty due to the initial conditions.

We consider both an Eulerian and a Lagrangian framework to analyse baroclinic wave activity. The first approach is based on the classic storm tracks (as defined by Blackmon 1976) and features an alternate bandpass-filter (Christoph et al. 1995), which has been applied in previous works to the ECHAM3 and ECHAM4 GCMs (e.g., Christoph et al. 1997; Ulbrich and Christoph 1999; Knippertz et al. 2000). The second approach is based on an automatic tracking algorithm (originally by Murray and Simmonds 1991; Simmonds et al. 1999), which was adapted to NH conditions by the authors (Pinto et al. 2005), and has previously been used to assess cyclonic activity in several GCMs (Leckebusch and Ulbrich 2004; Pinto et al. 2006; Leckebusch et al. 2006).

Based on the ECHAM5/MPI-OM1 scenario experiments, the main issues addressed are as follows: (a) Is synoptic activity significantly changed by increasing GHG forcing? (b) Are these changes sensitive to the choice of scenario experiment (and run)? (c) Are these changes associated with alterations in the NH mean flow? (d) Will they imply large (regional) changes in windstorm events?

The structure of the paper is as follows: Sect. 2 includes a description of the GCM and the model experiments; Sect. 3 describes the used methodologies; Sect. 4 includes results for the present climate conditions and validation against reanalysis data; Sect. 5 considers the three climate change scenario experiments and relates the observed changes to the NH general circulation and regional impacts. A short discussion concludes the paper.

2 Data

This study is based on climate experiments performed with the coupled GCM ECHAM5/MPI-OM1. The atmospheric model has a spatial resolution of T63 (63 spectral modes, triangular truncation, corresponding to a resolution of 1.875°), and 31 vertical levels up to 10 hPa (Roeckner et al. 2003). The ocean/sea ice model has a resolution of 1.5°, with conformal mapping

grid over the poles, and 40 vertical levels (Marsland et al. 2003). The model does not employ flux adjustments. General model descriptions, details concerning the coupling between atmosphere and ocean/sea ice models and included parameterisations can be found in Roeckner et al. (2003), Marsland et al. (2003) and Jungclaus et al. (2005). Roeckner et al. (2006) have emphasized the advantages of the choice a high vertical resolution for a realistic representation of the atmospheric circulation at T63. For our investigations, surface and pressure level data are used at full horizontal resolution (Gaussian grid correspondent to 1.875°) and at 6 hourly time step. The daily maximum 10 m wind speed (considered in Sect. 5) is based on the internal time step of the atmospheric model (15 min).

A total of 13 simulations are considered. The first one is the pre-industrial run (500 years with fixed 1860 GHG concentrations) as a pure control simulation. We have closely looked at the complete 500 year control run and found no evidence for a significant climate trend in the mean strength of the North Atlantic (NA) and the North Pacific (NP) storm tracks nor on global mean near surface temperature, though inter-decadal variability is present. Bengtsson et al. (2006a) concluded that the variability observed in this simulation is fundamentally a consequence of (natural) internal fluctuations of the climate system. The three runs for the recent climate (denominated 20C) were initialised at different states of this pre-industrial control simulation, and are forced with the historical GHG and aerosol concentrations for the period 1860–2000 (CO_2 concentrations change from 286 to 367 ppm). Natural external forces like volcanism and changes in solar activity were not considered. As no trends were detected in the pre-industrial run (see above), the three simulations are starting from different realisations of the same basic climate mean state. Additionally, there is no evidence that the historical realisations drift into different climate states. Therefore, we can postulate that internal variability is the main factor that produces the spread between results of the three realisations.

Additionally, we consider climate change experiments for three SRES scenarios (Nakićenović et al. 2000) for the twenty-first century (2001–2100): B1, A1B and A2. The CO_2 concentrations increase from 367 ppm (year 2000) to 540, 703 and 836 ppm by the year 2100 for scenarios B1, A1B and A2, respectively. Three realisations are considered per scenario, which were started with the final state of each of the three 20C runs. Therefore, they can be considered extensions of the previous runs. Again, given that no climate drift was found in the control run, and the three realisations for the same scenario show a comparable evolution of the global climate (e.g., near surface temperature), it can be assumed that observed changes in these climate change experiments may only be derived from the different GHG forcing and/or internal variability (this will be further explored in Sect. 5).

Finally, we use the NCEP-Reanalysis (Kalnay et al. 1996, hereafter NCEP) for the period 1958/1959–1997/1998 to validate the GCM results, considering both surface and pressure level data. The spectral horizontal resolution of the numerical model (T62) and temporal resolution (6 h) are the same as the GCM. Because of this characteristic, we preferred to validate the model results against the NCEP rather than the newer ERA40 data as it allows us to retain the methodology settings and disregard data resolution inconsistencies.

For all investigations, the analysis period is the winter half year (October to March). This option is motivated by the fact that there are frequent wind storm events affecting, e.g., Western Europe occurring in late autumn and early spring. Therefore, these periods are considered in our analysis. However, results for December to February are largely equivalent to those presented here (see also Sect. 6). Climate signal refers to the changes between end of the twenty-first century (2060–2100) and recent climate conditions (1960–2000). In Sect. 5, the complete runs (1860–2100) will be considered in some investigations.

3 Investigation methods

As indicated above, we consider both an Eulerian and a Lagrangian framework to analyse synoptic scale variability. The first approach was introduced by Blackmon (1976) and is defined as the standard deviation of the bandpass filtered variability of the 500 hPa height field and is commonly referred to as ''storm tracks''. Wallace and Gutzler (1981) and Blackmon et al. (1977, 1984a, b) later demonstrated that these are in fact westward propagating barocline waves. This variable is a widely accepted measure of synoptic activity and is highly adequate to analyse long GCM simulations. This assumption is supported by innumerable studies on baroclinic wave activity in GCMs (e.g., Stephenson and Held 1993; Hall et al. 1994; Lunkheit et al. 1996; Beersma et al. 1997; Ulbrich and Christoph 1999; Knippertz et al. 2000; Kushner et al. 2001; Chang and Fu 2002; Yin 2005).

We compute storm track activity bandpass-filtered 500 hPa geopotential height standard deviation following Christoph et al. (1995). The applied Murakami filter is a second order bandpass filter featuring forward and reverse recursion filtering. Its maximum amplitude

response is close to 4 days and the cut-off periods are 2.5 and 8 days (cf. Christoph et al. 1995, their Fig. 1). When climatological means are considered, the Murakami filter retains in general more variability than the Blackmon filter, while the field structures obtained with both techniques coincide well (Christoph et al. 1995). The storm track variable also includes some variability associated with high-pressure systems (which typically have longer time scales).

The second approach identifies and follows systems individually from their genesis to their dissipation. Even though these methods typically work with low level or ground data (unlike storm tracks), they also provide a good representation of synoptic scale activity. A general review of pertinent literature regarding tracking methodologies and their application to reanalysis data and GCM can be found, e.g., in Pinto et al. (2005, 2006) and is therefore not repeated here. Cyclones are identified and tracked based on mean sea level pressure (MSLP) using the objective method originally by Murray and Simmonds (1991) and Simmonds et al. (1999), which is organized in two steps. Firstly, cyclones are identified with an algorithm based on the search for the maximum of the Laplacian of the mean sea level pressure (denoted $\nabla^2 p$, which is equivalent to seek for extremes of the relative vorticity) and its location attributed to the correspondent pressure minima. Systems localized in areas with a terrain-height above 1,500 m above sea level are excluded (as being possible errors due to underground extrapolation of MSLP). Only systems whose circulation exceeds a minimum threshold value of $\nabla^2 p$ are considered (cf. Pinto et al. 2005, for further details). Secondly, the tracking algorithm is applied, which takes into account the most probable shift of the cyclone core under the given situation. Only systems with a minimum lifetime of at least 24 h are retained. The choice of 24 h (instead of a longer period) aims at leaving the shorter-lived cyclones in secondary storm track areas and secondary cyclones over the main oceanic basins in the statistics. Moreover, the cyclone must have reached a ''mature state'' at some point during lifetime (class 00, i.e., closed system featuring a true pressure minima and an $\nabla^2 p$ value larger than 0.6 hPa/(deg.lat)^2, cf. Pinto et al. 2005, their Table 2). For a detailed explanation on the current settings of the algorithm and its implications refer to Pinto et al. (2005). The variables regarded here are cyclone track density (number and length of cyclone tracks), cyclone intensity (averaged $\nabla^2 p$) and intensity tendencies (averaged $d\nabla^2 p/dt$), computed over a 7.5° radius for each gridpoint.

A note regarding the complementarities of the two methods: while the classic storm track approach permits a fast coverage of large amounts of data and is a very robust variable (hardly sensitive to the settings unlike cyclone tracking), the cyclone track approach permits the analysis of individual systems, and hence of genesis, -lysis, lifetime, and intensity statistics. Moreover, the assessment of frequency distributions in terms of cyclone strength and the analysis of extremes are possible. The Eulerian approach is applied to mid-tropospheric geopotential height fields, whereas the Lagrangian method uses surface as input data. Hence, the conjunction of both methods enables the assessment of baroclinic waves in their diverse forms of ''manifestation''.

4 Synoptic activity in the present climate

In this section, storm tracks and cyclone statistics derived from the ECHAM5 simulations for recent climate conditions (ensemble average, years 1960–2000, referred to as 20C) are presented and validated against NCEP (1958–1998). Based on its comparison it will become evident that the GCM is able to reproduce the main patterns of quantities considered for synoptic activity, while beyond the general agreement some deviations can be identified. Figure 1a, b show the storm track for 20C and for NCEP, respectively. The two elongated high-activity areas over the NA and NP will be hereafter be referred to as the ''NA storm track'' and ''NP storm track'', respectively. In comparison to the NCEP, the GCM shows more a zonal storm track over the Eastern NA and Western Europe, while the NP storm track is stronger and located slightly further north and downstream. Cyclone track density can be found in Fig. 1c for the 20C and Fig. 1d for NCEP. In comparison to the storm tracks (Fig. 1 a, b), the cyclone track density (Fig. 1c, d) shows a more southwest-northeast orientation (particularly over the NA) and their centres are displaced downstream compared to those from the storm track. GCM and NCEP cyclone statistics are in rather close agreement (Table 1, see also Pinto et al. 2005, their Fig. 6), even though simulated cyclone track density is somewhat smaller than its NCEP counterpart at high latitudes, and more intense over the central and eastern NA (cf. Fig. 1c, d). Over the western NP mid-latitudes, the cyclone tracks are shifted northeast.

In terms of intensity tendencies, an intensification of systems is found near and downstream of the NA and NP baroclinic zones (Fig. 1e, f). Thick black lines in Fig. 1e, f denotes baroclinicity, defined as the maximum Eady growth rate at 400 hPa (cf. Hoskins and Valdes 1990). Decreasing intensities are typical of continental areas located downstream. There is a good

Table 1 Cyclone counts in NCEP and ECHAM5 for selected regions

Regions	NCEP (N)	20C (N, %)	B1 (N, %)	A1B (N, %)	A2 (N, %)
CNA	571.9	606.3 (+**6.1%**)	572.0 (**–5.7%**)	561.9 (**–7.3%**)	560.5 (**–7.6%**)
CNP	825.8	786.1 (**–4.8%**)	756.2 (**–3.8%**)	746.9 (**–5.0%**)	733.9 (**–6.6%**)
WEU	179.3	218.9 (+**22.4%**)	206.5 (**–5.7%**)	207.1 (**–5.4%**)	204.9 (**–6.4%**)
MM	230.3	206.3 (**–10.4%**)	184.1 (**–10.8%**)	176.9 (**–14.3%**)	175.5 (**–14.9%**)
NH	5,218.4	5,047.1 (**–3.3%**)	4,859.7 (**–3.7%**)	4,795.2 (**–5.0%**)	4,770.3 (**–5.5%**)

Total cyclone counts per winter (N) for selected areas over the NH (ensemble averages)

Row (a): CNA (b): CNP (c): MM. (d) WEU. These areas are drawn in Fig. 1a and 3d. (e) Northern Hemisphere 20°–85°N. Significant differences at 95% (and 99%) confidence levels are in bold (and underlined), t-test on winter basis

Table 2 Changes in cyclone intensities for selected regions

Regions	$\nabla^2 p$ [hPa/(deg.lat)^2]	20C (N)	B1–20C (%)	A1B–20C (%)	A2–20C (%)
CNA	<0.8	232.0	**–5.3**	**–6.5**	**–7.3**
	0.8–1.5	233.5	**–6.0**	**–7.8**	**–8.3**
	1.5–2.5	118.1	**–5.9**	**–8.3**	**–7.4**
	>2.5	22.8	–4.7	–6.2	–3.4
CNP	<0.8	296.1	–0.6	–0.7	**–2.5**
	0.8–1.5	287.0	**–6.1**	**–7.5**	**–9.6**
	1.5–2.5	159.3	**–5.4**	**–8.2**	**–9.2**
	>2.5	43.7	–4.3	**–4.9**	**–5.5**
WEU	<0.8	87.6	**–5.9**	**–7.0**	**–8.7**
	0.8–1.5	85.1	**–7.1**	**–7.3**	**–8.7**
	1.5–2.5	39.0	–3.6	0.0	-0.2
	>2.5	7.1	+2.7	+7.4	+**14.8**
MM	<0.8	155.9	**–7.9**	**–10.5**	**–10.3**
	0.8–1.5	46.7	**–19.5**	**–25.5**	**–28.5**
	1.5–2.5	3.7	**–21.9**	**–30.4**	**–37.5**
	>2.5	0.0	–	–	–

Cyclone counts per winter determined for four classes in terms of intensity ($\nabla^2 p$ values) and presented selected areas over the NH (ensemble averages). Cyclone counts (N) are calculated 0.1 hPa/(deg.lat.)^2 segments

Row (a): CNA (b): CNP (c): MM. (d) WEU. These areas are given in Fig. 1a and 3d. Within each area, changes in cyclone counts for each intensity classes are given in percentage. Significant differences at 95% (and 99%) confidence levels are in bold (and underlined), t-test on winter basis

agreement of 20C and NCEP climatologies (Fig. 1e, f), though the GCM intensification rates are lower in some areas, e.g., at the entrance of the NA storm track and south of Greenland, and higher at lower latitudes over the eastern NA and southwest Europe. Over the NP, intensification rates are reduced south of Japan and increased over Eastern Asia/Japan and south of the Aleutian Isles (cf. Fig. 1 e, f). Maxima of cyclone intensities (measured as $\nabla^2 p$, Fig. 1g, h) are found north-eastward of the NA and NP storm track maxima (cf. Fig. 1a, b) and near the corresponding areas of maximum cyclone track density (cf. Fig. 1c, d). GCM cyclone intensities are somewhat lower than their NCEP counterparts, while intensities between Greenland and Scandinavia and over the higher latitudes of the NP are larger (cf. Fig. 1g, h). These deviations could be expected from the differences in cyclone track density and storm tracks mentioned earlier in this section. In summary, we find an overall agreement of climatological patterns and underlying physical mechanisms between the GCM and NCEP.

Further, we compare the intensity distribution of cyclones on 20C and NCEP for main storm tracks (cf. areas in Fig. 1a): While again we find general agreement for both CNA (Fig. 2a) and CNP (Fig. 2b), there are some statistically significant (99% level according to a T-test) deviations with opposite signature over the two basins. A smaller share of intense cyclones [>1.5 hPa/(deg.lat)^2] is identified from the 20C runs compared to NCEP over the main NA storm track (Fig. 2a), while the opposite deviation is found for the NP (Fig. 2b). These differences are significant at the 99% significance level. The quantities are given in relative frequency of cyclone counts to take into account the different number of total counts found in both datasets (Table 1). Please note that the cut-off of the frequency at low intensities [below 0.7 hPa/(deg.lat)^2] is a consequence of the selection process

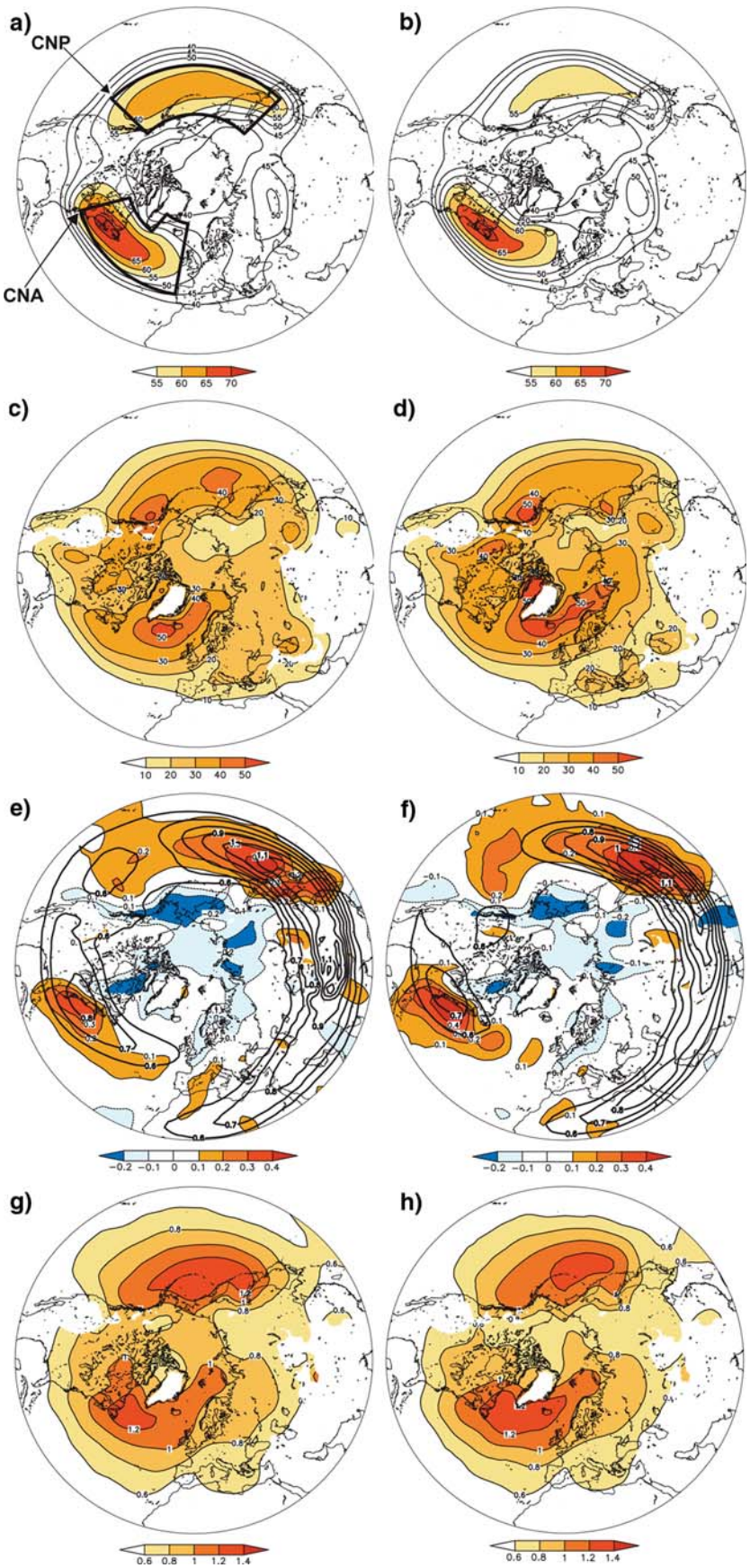

Fig. 1 Storm track and cyclone track statistics for ECHAM-20C (ensemble averages, 1960–2000) and NCEP (1958–1998) **a** storm track for 20C (interval: 5 [gpm]), **b** as **a** but for NCEP, **c** cyclone track density for 20C (interval: 10 [cyclone days/winter]), **d** as **c** but for NCEP, **e** intensity tendencies for 20C [$d\nabla^2 p/dt$, interval: 0.1 hPa/(deg.lat.)^2.day]. Also included is the upper-tropospheric baroclinicity field at 400 hPa (*bold lines*, interval 0.1 [1/day]. **f** As **e** but for NCEP, **g** cyclone intensity for 20C [$\nabla^2 p$, interval: 0.2 hPa/(deg.lat.)^2]. **h** As **g** but for NCEP. For **c**–**h**, *isolines* and *shadings* in areas with orography above 1,500 m are suppressed. The areas CNA (central North Atlantic) and CNP (central North Pacific) are defined in **a**

inherent to the method which excludes very weak systems. For more details please refer to Pinto et al. (2005, their Fig. 4).

The deviations for these areas documented above coincide closely with those present in the jet stream (which can be identified from the zonal wind at 250 hPa, cf. Figure 8 in Sect. 5) and upper-air baroclinicity in the GCM (Fig. 1e), which are indeed too zonal over the Eastern NA and Europe, and shifted North or Northeast over Western Asia/Japan and Eastern and Central NP (difference to NCEP not shown). The role of the jet stream for the storm track activity is explored in detail in Sect. 5 and 6.

5 Synoptic activity in a changed climate

In this section, storm tracks and cyclone statistics for the twenty-first century climate conditions are compared to the 20C results. Each GHG-forcing scenario (A1B, A2 and B1, respectively) is considered separately. The robustness of the obtained patterns is tested for the different forces, and the spread between the individual ensemble members is also considered. Further, links to alterations in the Northern Hemisphere mean flow are explored. The consistency of regional changes in cyclone intensities is addressed, together with impacts on the strong wind events.

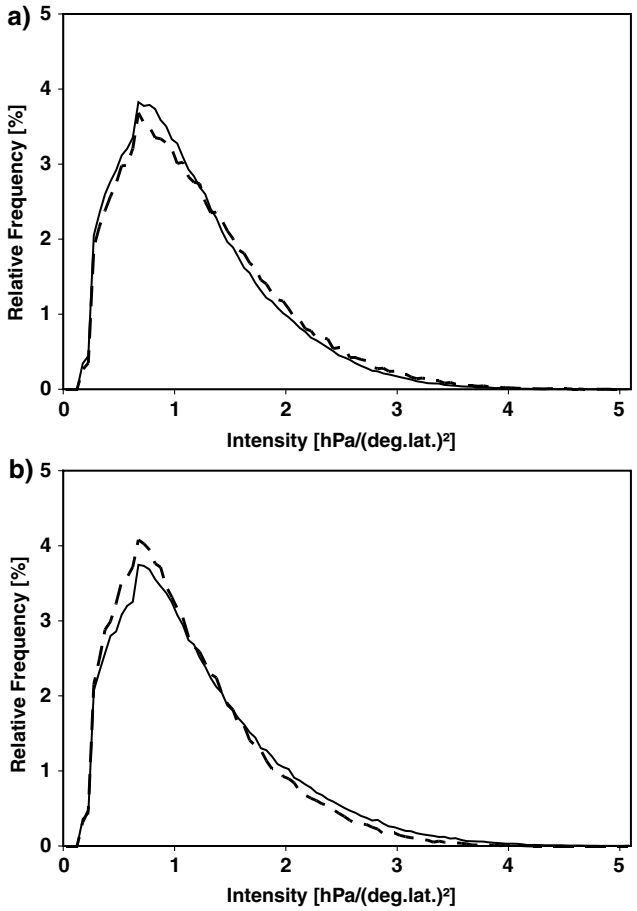

Fig. 2 Distribution of cyclone counts in terms of intensity ($\nabla^2 p$ values) for selected areas over the NH for ECHAM-20C (ensemble averages) and NCEP data. Cyclone counts displays are relative frequency (%) and calculated for 0.1 hPa/(deg.lat.)^2 segments. **a** CNA **b** CNP. These areas are defined in Fig. 1a. *Dashed black line* NCEP, *full black line* 20C

5.1 Changes in synoptic activity in the scenario experiments

Changes in ensemble mean storm track for the A1B experiment (Fig. 3a) feature an enhanced Atlantic storm track over the Eastern NA and Western Europe (+4.8 gpm, +8.5%), extending (with smaller enhancements) until the Pacific Siberian Coast. Over the Central NP, a spot of increased activity is found south of the Aleutian Isles (+2.4 gpm, +3.9%), while significant reductions are detected at lower latitudes and within the polar circle. At the same time, a significant reduction in cyclone track density can be observed for large parts of the NH (Fig. 3b), particularly strong at lower latitudes (e.g., Mediterranean), the NP Canadian Coastal area, north of Scandinavia and east of Japan (reaching about –6 cyclone days/winter). In areas with enhanced storm track activity (primarily the Eastern NA mid-latitudes, Fig. 3a) the reduction is small or even absent, but unlike expected (from the storm track results) there is no increase in local cyclone track density. However, other cyclone-related quantities, particularly the increased mean cyclone intensification rates and intensities e.g. over the eastern NA (Fig. 3c, d), do show signals that corroborate the changes in the mid-troposphere. The agreement of the patterns is, however, not tight. Increased intensification rates for the A1B ensemble (Fig. 3c) go well with changes in the upper-tropospheric baroclinicity (not shown) and match the signals in intensity (Fig. 3d) in some locations (e.g., enhanced intensification near Newfoundland and increased intensities west of Great Britain), even though the correspondence is not tight. Over the NP, little changes in cyclone intensity are found, even though intensification rates are enhanced over the central NP.

Table 1 clearly shows that the scenario runs produce a decreasing number of cyclone counts over the two basins (–7.3 and –5% for CNA and CNP, respectively), a result that is also valid for the whole NH (–5%). Moreover, Table 2 indicates that this reduction occurs irrespective of the intensity class considered. For the Mediterranean region (area defined in Fig. 3d, MM)

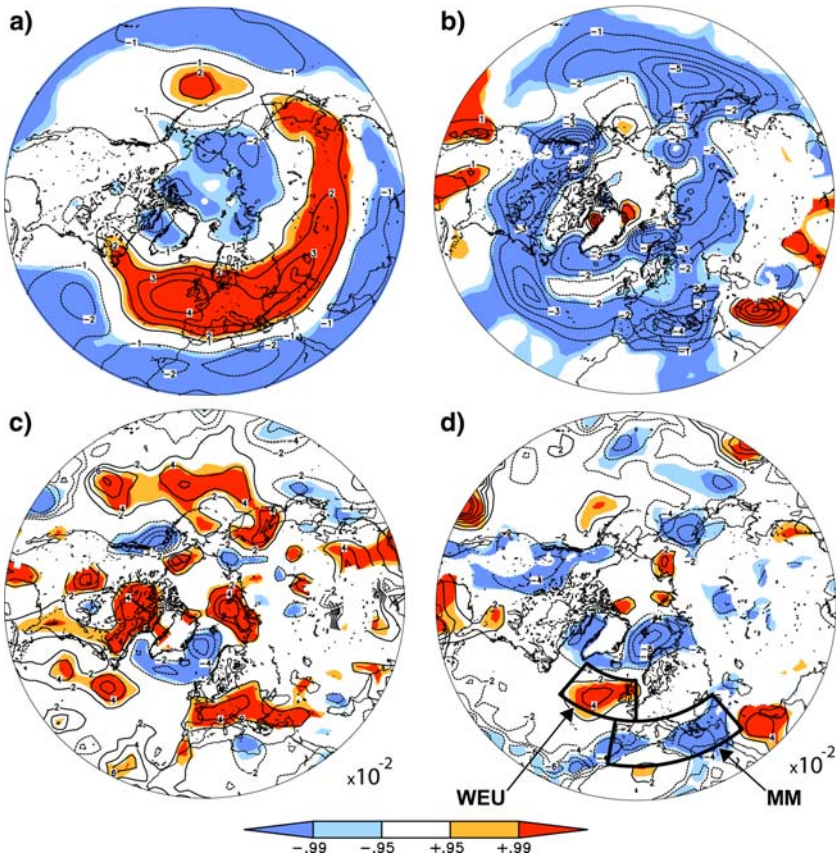

Fig. 3 Storm track and cyclone track statistics for ECHAM-A1B (ensemble averages, 2060–2100) **a** storm track for A1B minus 20C (interval: 1.0 [gpm]), **b** as **a** but for cyclone track density (interval: 1.0 [cyclone days/winter]) **c** as **a** but for intensity tendencies [$d\nabla^2 p/dt$, interval: 2×10^{-2} hPa/(deg.lat.)^2.day]. **d** As **a** but for cyclone intensity [$\nabla^2 p$, interval: 2×10^{-2} hPa/(deg.lat.)^2]. For **b**–**d**, *isolines* and *shadings* in areas with orography above 1,500 m are suppressed. Areas with significance differences (95 and 99% confidence levels) are in colour (t-test on winter basis). The areas WEU (Eastern North Atlantic and Western Europe) and MM (Mediterranean) are defined in **d**

the decrease is even stronger, amounting to –14% in total and about –30% for the strongest local cyclones [>1.5 hPa/(deg.lat)^2]. Note that, unlike for the main storm tracks, the weakest cyclones are here clearly less affected than stronger ones. A significant exception is the Eastern NA and Western Europe (area defined in Fig. 3d as WEU): the number of the most intense cyclones [>2.5 hPa/(deg.lat)^2] increases (though it misses 95% confidence level significance marginally), while the number of weaker cyclones decreases.

The storm track ensemble mean for the A2 runs shows significant enhanced values over the NA, central Asia and NP, with an absolute increase of +5.7 gpm (+10.6%) west of Britain (Fig. 4a). Changes in cyclone track density (Fig. 4b) also show a widespread reduction of activity over all main areas and the Mediterranean (reaching about –5 cyclone days/winter, cf. also Table 1). The general patterns are similar to those of A1B (Fig. 3a, b), but with larger loadings and, in the case of the storm track, extending further downstream over the NP. In terms of changes in cyclone intensity and intensification rates, results include the largest relative changes in comparison to 20C (not shown), e.g., with a significant enhancement of number of most intense cyclones for WEU of about +15%, and a reduction of the strongest local cyclones for MM of about 38% (cf. Table 2), which confirms findings from recent studies (e.g., Leckebusch et al. 2006).

The results for the B1 simulations show, as expected, the weakest changes in comparison to 20C for all three climate experiments. The storm track changes are negligible over the NP (cf. Fig. 4c), while over the NA the signal reaches only +3.6 gpm (+6.7%). Nevertheless, cyclone track density is still significantly reduced over most areas (Fig. 4d). Changes in cyclone intensity are neither significant south of the Aleutian Isles nor west of Great Britain (not shown), even though significant results are obtained for some intensity classes (Table 2).

5.2 Robustness of the synoptic scale changes

Comparing the three experiments, results show a high coherence in terms of geographical patterns, and the detected loadings of these patterns are typically the strongest (weakest) for the experiment with the largest (lowest) GHG forcing. Hence, they fulfil the expectations, even though there is clearly some non-linearity in the results. Of note is the fact that the climate signals for the storm track ensemble means (cf. Fig. 3a, 4a, c) display their major changes not over the main storm track areas but rather further downstream (exit regions). The

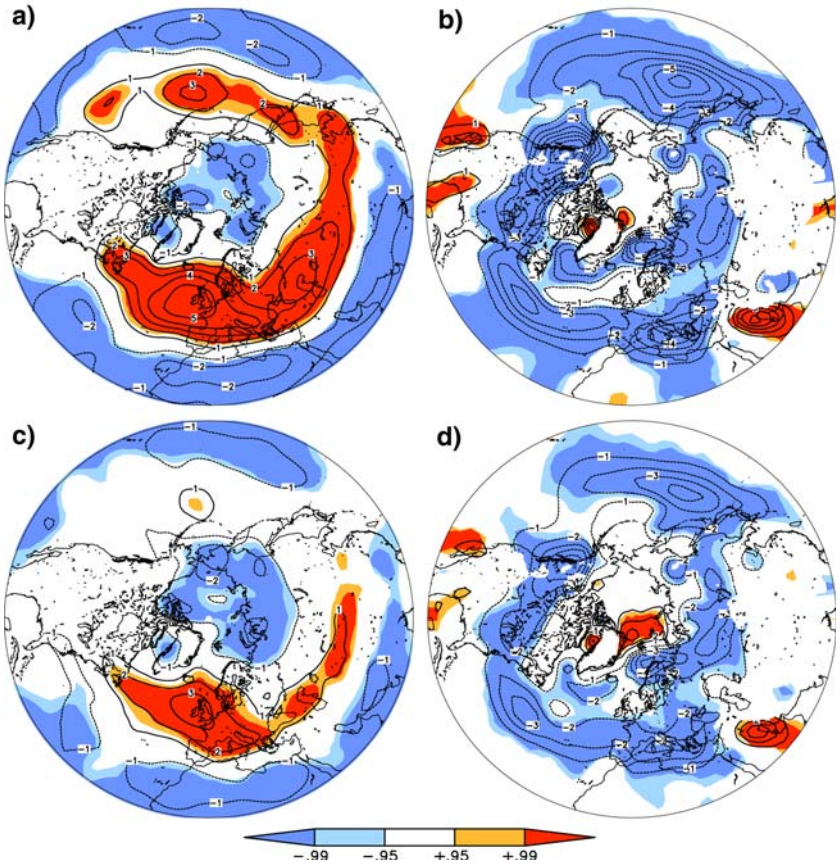

Fig. 4 Storm track and cyclone track statistics for ECHAM-A2 and B1 (ensemble averages, 2060–2100) **a** storm track for A2 minus 20C (interval: 1 [gpm]), **b** as **a** but for cyclone track density (interval: 1.0 [cyclone days/winter]), **c** as **a** but for B1. **d** As **b** but for B1. For **b** and **d**, *isolines* and *shadings* in areas with orography above 1,500 m are suppressed. Areas with significance differences (95 and 99% confidence levels) are in colour (t-test on winter basis)

relevance of these climate signals was also tested against the spread between the single realisations for each scenario (approximated as the standard deviation). Results show strong indication of very stable results for the Eastern North Atlantic and Europe (where signals are large and the spread between the runs is small, in particular for A2), while for the NP the signals are weaker (figure not shown). This aspect can be seen most easily in Fig. 5, given the storm track changes for the three A1B ensemble members. They agree in producing the largest signals downstream of the Atlantic storm track maximum, with an extension into the Asian continent, and a spot of increased activity over the NP. Here, the patterns agree less over the Eastern NP/Asia, and the significant changes in the ensemble mean (Fig. 3a) are largely derived from run one alone.

In terms of the distribution of cyclone intensities for the main storm track areas, results for the three scenarios agree that the distributions remain fairly similar to those of 20C, as relative changes are similar for different intensities (cf. Table 2). However, this is not the case for all regions in the NH, as, e.g., in the MM intense cyclones are particularly affected by the changed climate, and for WEU a shift to more intense systems is detected.

Further, we analyse the sensitivity of the two main storm tracks to the prescribed forcing. Considered now are time series of ensemble mean storm tracks averaged over the main areas (boxes in Fig. 1a) for the complete simulations. Values are given in 11 year running means for 20C, B1, A1B and A2 (Fig. 6a, b). The periods considered in the previous figures are indicated (1960–2000 and 2060–2100). Also included are the average value correspondent to the 500 year pre-industrial simulation (where no significant long-time trend in storm track activity could be identified, cf. Sect. 2) and its standard deviation (1–3 σ). We find evidence for the link between increased GHG forcing and storm track activity: The curves for the three climate simulations drift from the pre-industrial mean state to enhanced values, exceeding, e.g., $+2\sigma$ for A2 by the end of the twenty-first century (2σ corresponds roughly to the 95% percentile, i.e., beyond what could be considered ''natural internal variability''). This result is valid for both ocean basins. As an additional test, the bootstrap method (which is independent from the distribution) is used: 1,000 synthetic time series were created based on the 500 year pre-industrial run. Next, 40 year running means were computed for the NA and NP storm track areas (as defined in Fig. 1a). Finally, it

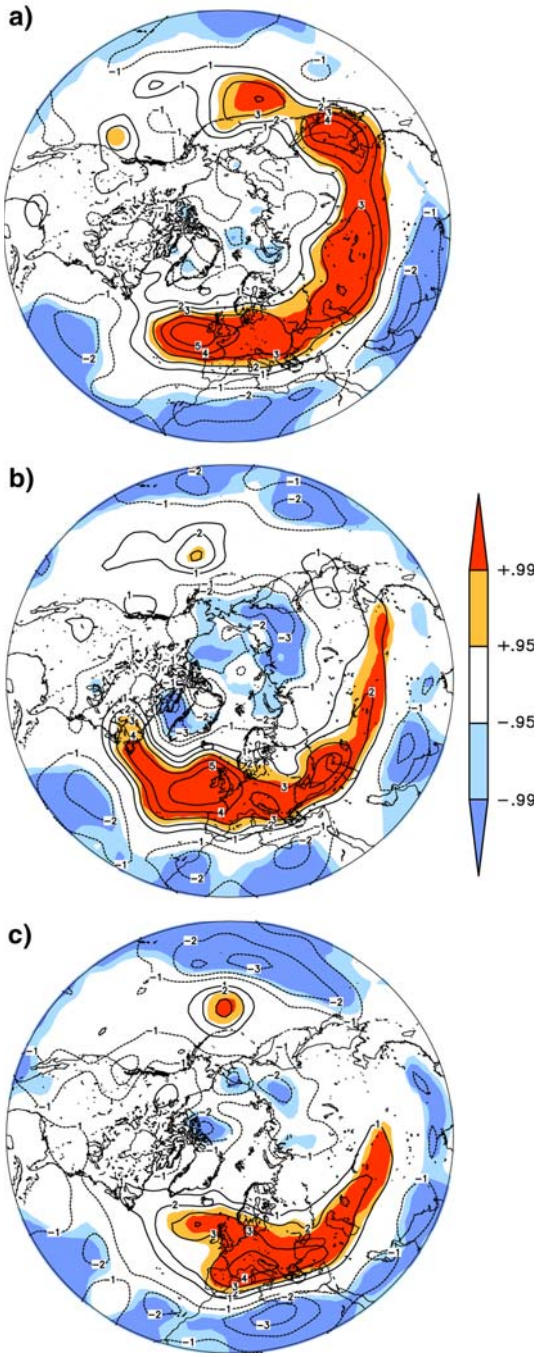

Fig. 5 Storm track statistics for ECHAM-A1B (three runs, 2060–2100) **a** storm track for A1B minus 20C for the first run (A1B.1 vs. 20C.1, interval: 1.0 [gpm]), **c** same as **b** for the second run, **d** same as **b** for the third run. Areas with significance differences (95 and 99% confidence levels) are in colour (t-test on winter basis)

was tested if any of the 1,000 artificial storm track intensity series generated from the pre-industrial run included 40 year (running mean averaged) periods which were at least as high as that of 2060–2100 for the respective (NA or NP) storm track. This was not the case. This additional test confirms that the NA and NP storm track intensities over this last segment of the twenty-first century are outside the range of variability of the pre-industrial climate simulation. Regarding the twentieth century, the 1960–2000 average for the NA storm track is close to the pre-industrial average (and is detected quite often in the 1,000 synthetic time series), while NP storm track average is already outside the range of variability of the pre-industrial run. This may partly explain why the climate change diagrams for the NP storm track area (cf. Fig. 3a, 4a, c) show little significance of results when comparing the periods 2060–2100 to 1960–2000 (see also Sect. 6).

5.3 Links to alterations in the NH mean flow

In this subsection, we compare the changes detected in storm track and cyclone activity with alterations of the large-scale atmospheric circulation over the NH in the GCM. We analyse the North Atlantic Oscillation index (NAO), which is associated with north–south displacements of the NA storm track (e.g., Rogers 1990; Hurrel 1995), the blocking index (Tibaldi and Molteni 1990), which accounts for the zonality of the NH mid-latitude flow, and the jet stream, which controls the position, location and the growth rate of barocline waves (e.g., Nakamura 1992; Christoph et al. 1997).

The increased synoptic activity over the NA is associated with an increased NAO-index (e.g., Hurrel 1995). The index was calculated as the normalised pressure difference between Iceland (averaged for 0°–40°W; 55°–70°N) and Azores (averaged for 0°–40°W; 35°–50°N). Figure 6c shows an 11 year running mean for the ensemble average of the experiments. In order to make the indices comparable, they have been computed using the same mean and normalisation factors, which are based on all simulations. Note that this NAO index is correlated with NA average storm track (Fig. 6a) with a value of 0.74 for the ensemble average 20C plus A1B (black and red curve, for B1 and A2 the values are similar). Therefore, and comparable to the NA storm track values, the NAO indices drift away from values close to the pre-industrial mean state at the end of the twentieth century and remain in a positive phase during most of the twenty-first century, even exceeding 3σ for A2 (correspondent roughly to the 99.7% percentile). Further analysis (via EOF studies) showed indication of a north-eastward shift of the NAO centres of action in the scenario experiments, similar to the findings of Ulbrich and Christoph (1999), but this aspect will be left for future research.

Given this result, we further explore changes in the atmospheric circulation for the whole NH. With this

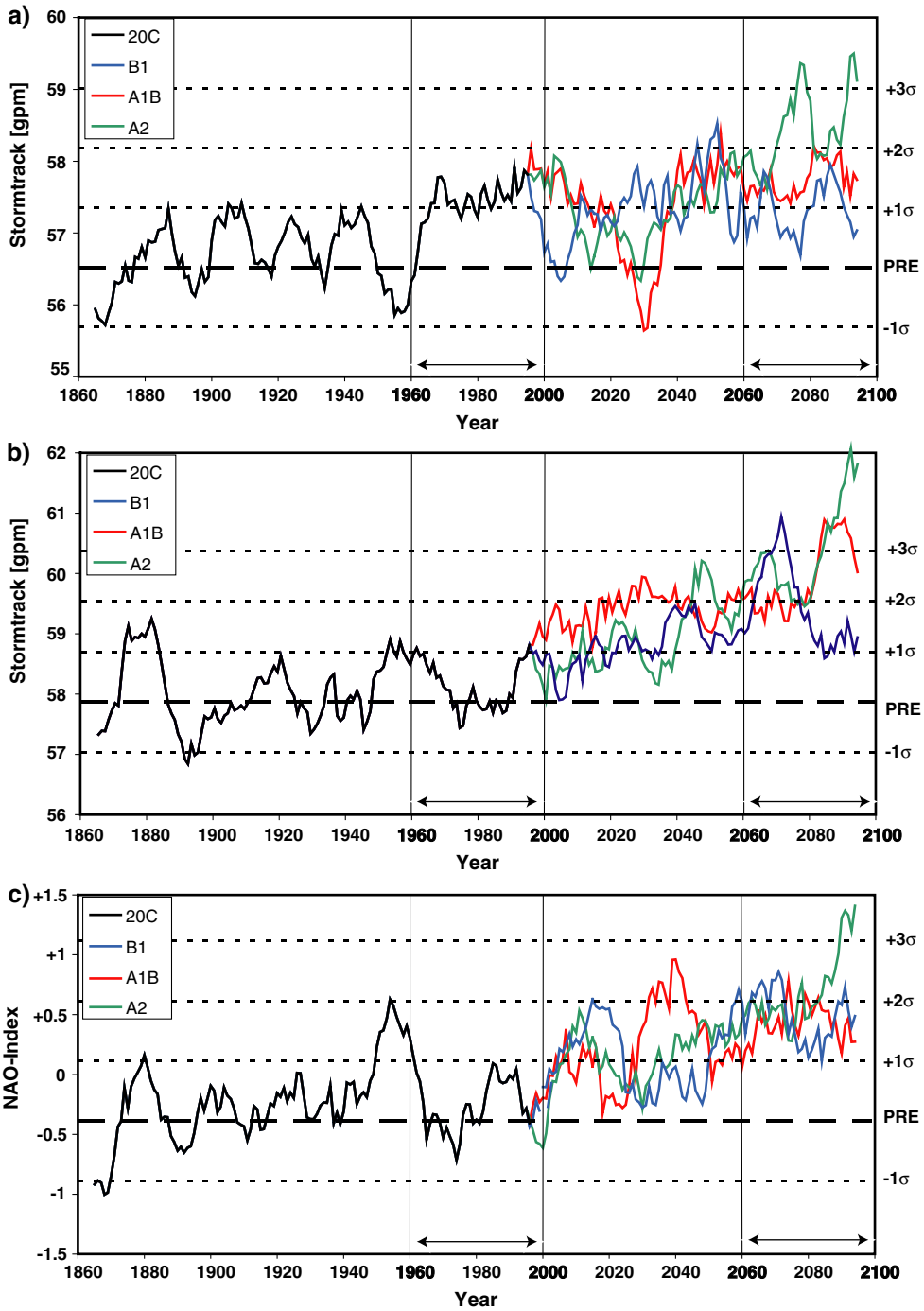

Fig. 6 Changes in area averaged storm track activity and NAO index for the complete runs (ensemble averages, 1860–2100). **a** Area averaged storm track for the North Pacific [gpm], data presented as 11 year running means. *Black line* 20C, *blue line* B1, *red line* A1B, *green line* A2. The average values and standard deviation for the control run are given as reference. 1σ, 2σ and 3σ correspond to the 68.3, 95.5 and 99.7% percentiles, respectively. **b** Same as **a** but for the North Atlantic, **c** NAO index calculated based on normalized pressure anomalies between [0°–40°W; 35°–50°N] and [0°–40°W; 55°–70°N] on winter basis. Data presented as 11 year running means. The areas for **a** and **b** are defined in Fig. 1a. The periods 1960–2000 and 2060–2100 are indicated in all *panels*

aim, we analyse the frequency of atmospheric blocking, which has been long recognised as a physical process of profound dynamical interest and of great practical relevance for operational forecasts (Tibaldi and Molteni 1990; and references therein). The simple blocking index by Tibaldi and Molteni (1990) is used. Results for B1, A1B and A2 (blue, red and green curves in Fig. 7) show clear indication of a more zonal circulation (less blocking), notably over the NA/Europe (60°W–35°E) and over the NP (130°–220°E) in comparison to 20C (black line). As expected, changes are largest (smallest) for the scenario with the higher (lesser) GHG-forcing A2 (B1) for most longitudes. The largest changes can be observed over the NA storm track core (around 50°W) and go well with extension of the NA storm track into Europe (Fig. 3a) and the shift of the NAO-index to more positive values (Fig. 6c). Note the very close agreement between the

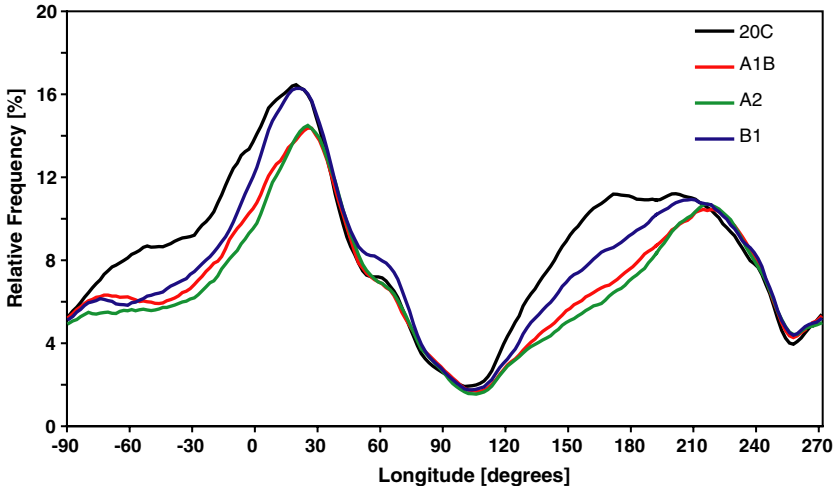

Fig. 7 Blocking index for the Northern Hemisphere mid-latitudes (ensemble averages). Values computed on a daily basis and given as relative frequencies versus longitude. *Black line* 20C, *blue line* B1, *red line* A1B, *green line* A2

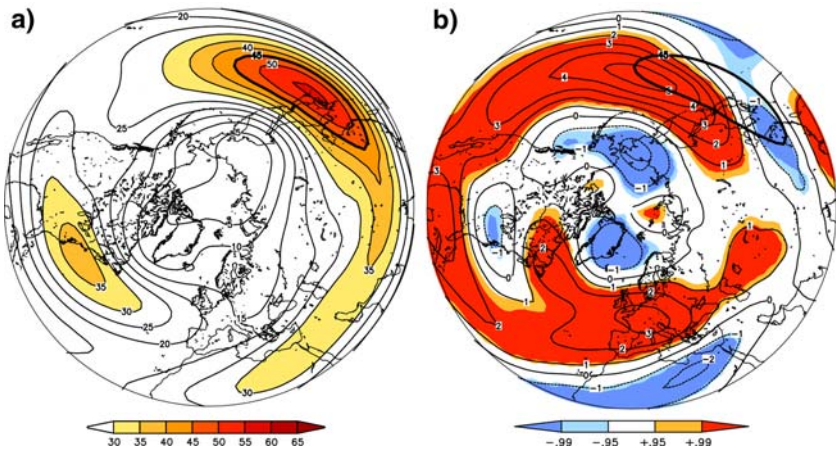

Fig. 8 Jet Stream (zonal wind component) for 250 hPa geopotential height (ensemble averages). **a** Mean field for 20C (interval: 5.0 [m/s]), **b** A1B minus 20C (interval: 1.0 [m/s]). The *isolines* correspondent to 45 m/s are marked in thick lines: on panel, **b** this *isoline* corresponds to the ECHAM-A1B ensemble average. For **b**, areas with significance differences (95 and 99% confidence levels) are in colour (t-test on winter basis)

three scenario curves over the NA, which is maintained further downstream (up to central Europe, 30°E) for the A1B and A2 curves.

The changes in storm tracks and blocking frequencies are associated with changes in the jet stream, defined as the zonal wind component at 250 hPa (Fig. 8a). The climate change signal over the NP (depicted for the A1B scenario in Fig. 8b) shows a northward broadening at the longitudes of the jet maximum, as well as a downstream extension at the longitudes of the strongest blocking changes (Fig. 7). Local increases reach +5.4 m/s (+13%) west of Japan. Over the NA area, changes are weaker in absolute terms, but similar in structure: There is a broadening around the jet stream's core, and a downstream extension into Western Europe (locally up to +20%). Simultaneously, the North African entrance of the subtropical jet stream is weakened. These changes in the mean circulation are observed for all scenario simulations and ensemble members (with various loadings), and go well to the eastward shift in the storm tracks discussed earlier, indicating that they are only part of a more general change of the NH atmospheric circulation under enhanced GHG forcing.

5.4 Changes in strong wind events

Within the context of climate change, it is important to analyse the impact of altered cyclone intensities over the most affected regions. Of particular interest is the area over Eastern North Atlantic and Western Europe (WEU), where a clear shift to more intense cyclones [>2.5 hPa/(deg.lat)^2] was detected (Table 2), even though the total number of counts is reduced by 5% (Table 2). In order to assess the regional impacts of these changes, we analyse the climate signal of a high percentile (98%) of the local wind climatology (Fig. 9a) in terms of daily maximum 10 m wind. This percentile is chosen as it is assumed to correspond to the threshold for local wind speeds to produce damage (Klawa and Ulbrich 2003). Compared to NCEP, maximum wind values in the GCM are typically larger over

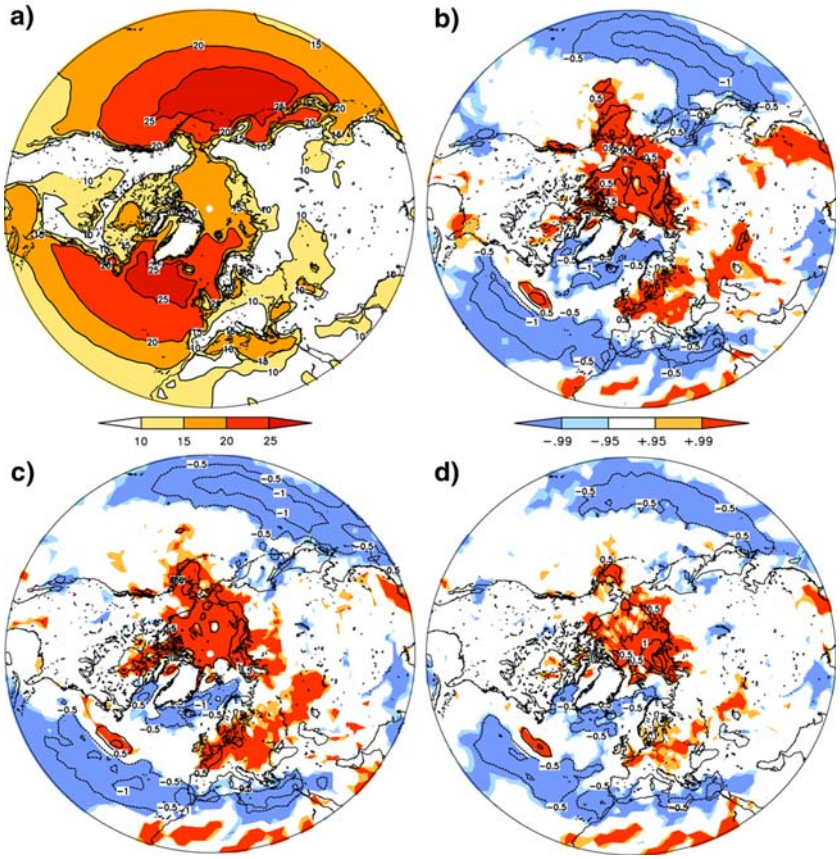

Fig. 9 Ninety-eight percent-percentile of maximum daily 10 m wind (ensemble averages). **a** Mean field for 20C (interval: 5.0 [m/s]), **b** A1B minus 20C (interval: 0.5 [m/s]). **c** A2 minus 20C (interval: 0.5 [m/s]). **d** B1 minus 20C (interval: 0.5 [m/s]). *Isolines*, values and shadings in areas with orography above 1,500 m are suppressed. For **b–d**, areas with significance differences (95 and 99% confidence levels) are in colour (t-test on winter basis)

the main ocean basins (in particular over the main storm tracks) and lower over continental areas, particularly over high orography. Over the main ocean basins, the negative changes between the recent and future climate for the A1B, A2 and B1 (Fig. 9b–d, respectively) are significant at lower latitudes over the NA and NP (only over western and central parts). Please note that over most of the NP storm track (particularly its eastern part) hardly any changes are detected. Over the Polar Regions, positive signals are found, as well as over parts of Europe and Far East Asia. Note the good agreement between these figures and those for storm track and cyclone intensities shown above, as they occur typically further downstream. The signals are, as expected, largest (smallest) for the A2 (B1) runs. These anomalies are spatially coherent for all higher percentiles (90–99.9%) and point towards more extreme and/or frequent wind storms over these areas, in particular for parts of Europe.

In summary, we have found evidence that the alterations in synoptic activity detected in the ECHAM5 simulations (a) are significant over large areas of the NH mid latitudes irrespective of the climate experiment for twenty-first century (b) show differences in intensity depending on the scenario (c) are associated with alterations of the NH circulation and background conditions (blocking frequencies, NAO, jet stream) (d) are expected to imply large changes in windstorm events in some regions (e.g., parts of Western Europe).

6 Summary and discussion

We considered changes in synoptic activity in ECHAM5/MPI-OM GCM experiments both in terms of the Eulerian and the Lagrangian representations of synoptic scale activity (storm tracks at 500 hPa and surface cyclone tracks, respectively). The storm tracks are intensified over large areas of the NH mid latitudes at the end of the twenty-first century irrespective of the scenario experiments. The most affected areas are the eastern NA and Europe, where all scenarios and individual ensemble members produce similar patterns of change. Somewhat weaker increases are found for Asia, far-East and NP, where the agreement between individual patterns is smaller. At lower latitudes, wave activity is mostly reduced. At the same time, the number of cyclone tracks is significantly reduced over most of the NH. Note that the model's climate signal in

storm track and cyclone track statistics are different from the model's systematic deviations to NCEP. It is interesting to compare this result with both storm tracks and cyclone intensities (e.g., Fig. 3, 4) e.g., west of Great Britain: Although less synoptic systems (barocline waves) are present, they feature increased intensities (amplitudes) for this area. This assessment is supported by the enhanced counts found for more intense cyclones (cf. Table 2). Such an effect may also be valid for the region south of the Aleutian Isles, where a similar (but not significant) shift in distribution is found (data not shown).

These changes in storm track activity and cyclone intensities are linked with the increasing GHG-forcing, and even though they do not show a strict linear behaviour, they are largest (weakest) for the highest (lowest) forcing scenario. Even though the general tendencies of the climate signals are coherent, the variability between the individual runs may be over some areas as large as the differences between the ensemble averages (e.g., Eastern NP). The detected downstream shift of storm track activity is associated with lower blocking frequencies over the main ocean basins and an eastward shift of the polar front jet stream (and hence of baroclinic zones) by the end of the twenty-first century. These facts point to a possible change in the NH dynamics, in particular to a poleward shift of activity and the stronger zonal component of the mean flow. Not surprisingly, 11 year running means of area averaged values for the main storm tracks show increased values at the end of the twenty-first century, exceeding $+2\sigma$ (roughly correspondent to the 95% percentile) of the pre-industrial mean state in several cases. The impact on the long-term NAO phase is similar, showing a significant drift to a consistent positive phase with increasing GHG forcing.

Changes in storm track activity at the end of the twenty-first century are lower for the NP than for the NA, even though the increase in jet stream strength (and baroclinicity) are actually larger. One possible explanation for this is the fact that the NP storm track average (unlike the NA storm track) for 1960–2000 is already outside the range of variability of the pre-industrial run, possible due to both internal variability and non-linear response to the GHG-forcing. Another possible explanation is the phenomenon of mid-winter suppression of the NP storm track (Nakamura 1992), which has been observed for both observational and GCM data (e.g., Christoph et al. 1997). Among the mechanisms potentially leading to this phenomenon are the trapping of waves near the surface (e.g., Nakamura 1992) or the ''barotropic governor'' mechanism (e.g., James 1987). The negative feedback on the storm track occurs for jet velocities above a threshold around 44–45 m/s. Christoph et al. (1997) reported a more pronounced suppression with enhanced GHG forcing based on a previous version of the ECHAM model. The areas with jet velocities above 45 m/s are larger in the twenty-first century runs (cf. thick lines in Fig. 8), and the jet stream wind speed maximum exceeds 56 m/s suggesting that the same effect is present in the ECHAM5 scenarios considered here. A more detailed analysis is left for future work.

Our results are in general agreement with those presented by Bengtsson et al. (2006b). They considered the same ECHAM5 A1B experiment presented here but applied a different methodology for cyclone tracking. Their approach involves spatial and temporal filtering of the input data, and uses a different basic variable for obtaining the cyclone tracks, and a different vertical level (ζ 850 hPa). Their cyclone track density (Bengtsson et al. 2006b, their Fig. 2b) resembles sometimes more our storm tracks (also time filtered, our Fig. 1a) than our cyclone track density distributions (our Fig. 1b). The same is true for their climate signal (Bengtsson et al. 2006b, their Fig. 10a), which is in between our storm track and cyclone track density signals (Fig. 3a, b, respectively). Finally, our statistics are computed for October to March rather than December to February (DJF). This fact can largely be ruled out as a source of discrepancy, as our statistics for DJF feature basically the same patterns as the ones for the winter half year, only showing enhanced values/larger climate signals (not shown).

Considering other models, there is indication that a northward displacement of the NH storm tracks is a common feature in many twenty-first century GCM simulations (Yin 2005), which associated the detected signal with enhanced warming in the tropical troposphere, particularly for the upper levels. A northward shift of the storm tracks was also detected in our ECHAM4 investigations (Knippertz et al. 2000; Pinto et al. 2006), displaying larger signals and featuring a different climate change pattern in comparison to the ECHAM5 GCM. On the other hand, the present results show more agreement with those obtained with the HadCM3 simulations (Leckebusch and Ulbrich 2004; Leckebusch et al. 2006). A reduction in mid-latitude cyclone frequency (particularly for shallower cyclones) has also been observed by other authors (e.g., Geng and Sugi 2003). In particular, Leckebusch et al. (2006) gave evidence of a high agreement of the results between HadCM3, HadAM3P, ECHAM4 and ECHAM5 (one A2 simulation) for southern Europe, e.g., for the Mediterranean region. This gives indication that this pattern of change is not a model artefact.

Even though the distribution of mean cyclone intensities does not change considerably over the main storm track areas at the end of the twenty-first century, alterations are prominent over the Eastern NA/Western Europe. On the other hand, the reduction of activity at lower latitudes occurs particularly for the intense systems (shown for the Mediterranean basin). In spite of the different methodology, this result agrees with those obtained by Bengtsson et al. (2006b).

Finally, we explored the link between changed cyclone intensities and the higher percentiles of 10 m daily maximum wind and detected a close agreement, with prominent changes occurring typically further downstream. Previous work by the authors based on four different GCMs (Leckebusch et al. 2006) had already detected a significant increase in the occurrence of extreme winds over large parts of Europe by the end of the twenty-first century and explored their relationship with the 5% strongest cyclones. While the present results support their general results (with higher wind speeds over Britain, North Sea and Baltic Sea and nearby coastal regions, cf. Fig. 9), we also detected a very high sensitivity depending on the sample of simulations chosen, particularly in terms of regional results (e.g., Eastern NP). The reasons for this spread could be the low frequency variability in the simulations (not investigated here). Further analysis will be necessary to assess this uncertainty. Within our contribution to the ENSEMBLES project, the impact of climate change to several meteorological hazards and the associated physical mechanisms will be investigated, e.g., severe wind storms and floods. These studies will also consider regional models. A special emphasis is given to the European climate, and the ultimate aim is a risk assessment of the regarded meteorological hazards.

Acknowledgments This work was supported by the European Union Programme Energy, Environment and Sustainable Development under contract GOCE-CT-2003–505593-ENSEMBLES. We would like to kindly thank Erich Roeckner and the MPI for Meteorology (Hamburg, Germany) by order of the Federal Environment Agency for support and providing the ECHAM5 data and the DKRZ/WDCC (Hamburg, Germany) for computer capacity. We are thankful to Sven Ulbrich for help preparing some of the figures. The detailed comments of two anonymous reviewers helped to focus the manuscript and improve its clarity.

References

Barring L, von Storch H (2004) Northern European Storminess since about 1800. Geophys Res Lett 31: L20202, doi: 10.1029/2004GL020441, 1–4

Beersma JJ, Rider KM, Komen GK, Kaas E, Kharin VV (1997) An analysis of extra-tropical storms in the North Atlantic region as simulated in a control and $2 \times CO_2$ time-slice experiment with a high-resolution atmospheric model. Tellus 49A:347–361

Bengtsson L (1991) Advances and prospects in numerical weather prediction. Q J R Meteorol Soc 117:855–902

Bengtsson L, Hagemann S, Hodges KI (2004) Can climate trends be calculated from re-analysis data? J Geophys Res 109: D11111, doi: 10.1029/2004JD004536

Bengtsson L, Hodges KI, Roeckner E, Brokopf R (2006a) On the natural variability of the pre-industrial European climate. Clim Dyn 27:743–760

Bengtsson L, Hodges KI, Roeckner E (2006b) Storm tracks and climate change. J Clim 19:3518–3543

Blackmon ML (1976) A climatological spectral study of the 500 mb geopotential height of the Northern Hemisphere. J Atmos Sci 33:1607–1623

Blackmon ML, Wallace JM, Lau NC, Mullen SL (1977) An observational study of the Northern Hemisphere wintertime circulation. J Atmos Sci 34:1040–1053

Blackmon ML, Lee Y-H, Wallace JM (1984a) Horizontal structure of 500 mb height fluctuations with short, medium and long time scales. Atmos Sci 41:961–979

Blackmon ML, Lee Y-H, Wallace JM, Hsu H-H (1984b) Time variation of 500 mb height fluctuations with short, medium and long time scales. Atmos Sci 41:981–991

Chang EKM, Fu Y (2002) Interdecadal variations in Northern Hemisphere winter storm track intensity. J Clim 15:642–658

Charney JG (1947) The dynamics of long waves in a barocline westerly current. J Meteorol 4:135–163

Christoph M, Ulbrich U, Haak U (1995) Faster determination of the intraseasonal variability of stormtracks using Murakami's recursive filter. Mon Weather Rev 123:578–581

Christoph M, Ulbrich U, Speth P (1997) Midwinter suppression of Northern Hemisphere storm track activity in the real atmosphere and in GCM experiments. J Atmos Sci 54:1589–1599

Cubasch U, Meehl GA, Boer GJ, Stouffer RJ, Dix M, Noda A, Senior CA, Raper S, Yap KS (2001) Projections of future climate change. In: Houghton JT et al (eds) Climate change, 2001. Cambridge University Press, Cambridge, pp 525–582

Geng Q, Sugi M (2001) Variability of the North Atlantic cyclone activity in winter analysed from NCEP-NCAR reanalysis data. J Clim 14:3863–3873

Geng Q, Sugi M (2003) Possible change of extratropical cyclone activity due to enhanced greenhouse gases and sulfate aerosols—study with a high-resolution AGCM. J Clim 16:2262–2274

Hall NMJ, Hoskins BJ, Valdes PJ, Senior CA (1994) Storm tracks in a high-resolution GCM with doubled carbon dioxide. Q J R Meteorol Soc 120:1209–1230

Hodges KI (1995) Feature tracking on the unit sphere. Mon Weather Rev 123:3458–3465

Hodges KI (1999) Adaptive constraints for feature tracking. Mon Weather Rev 127:1326–1373

Hoskins BJ, Hodges KI (2002) New perspectives on the Northern Hemisphere winter storm tracks. J Atmos Sci 59:1041–1061

Hoskins BJ, Valdes PJ (1990) On the existence of storm tracks. J Atmos Sci 47:1854–1864

Hurrel JW (1995) Decadal trends in the North Atlantic Oscillation: regional temperatures and precipitation. Science 269:676–679

James IN (1987) Suppression of baroclinic instability in horizontally sheared flows. J Atmos Sci 44:3710–3720

Jungclaus JH, Botzet M, Haak H, Keenlyside N, Luo JJ, Latif M, Marotzke J, Mikolajewicz U, Roeckner E (2005) Ocean

circulation and tropical variability in the coupled model. ECHAM5/MPI-OM. J Clim 19:3952–3972
Kalnay E, Kanamitsu M, Kistler R, Collins W, Deaven D, Gandin L, Iredell M, Saha S, White G, Woollen J, Zhu Y, Leetmaa A, Reynolds B, Chelliah M, Ebisuzaki W, Higgins W, Janowiak J, Mo KC, Ropelewski C, Wang J, Jenne R, Joseph D (1996) The NCEP-NCAR 40-year reanalysis project. Bull Am Meteorol Soc 77:437–472
Klawa M, Ulbrich U (2003) A model for the estimation of storm losses and the identification of severe winter storms in Germany. Nat Hazards Earth Syst Sci 3:725–732
Knippertz P, Ulbrich U, Speth P (2000) Changing cyclones and surface wind speeds over the North-Atlantic and Europe in a transient GHG experiment. Clim Res 15:109–122
König W, Sausen R, Sielmann F (1993) Objective Identification of cyclones in GCM Simulations. J Clim 6:2217–2231
Kushner PJ, Held IM, Delworth TL (2001) Southern-Hemisphere atmospheric circulation response to global warming. J Clim 14:2238–2249
Lambert SJ (1988) A cyclone climatology of the canadian climate centre general circulation model. J Clim 1:109–115
Leckebusch GC, Ulbrich U (2004) On the relationship between cyclones and extreme windstorms over Europe under climate change. Glob Planet Change 44:181–193
Leckebusch GC, Koffi B, Ulbrich U, Pinto JG, Spangehl T, Zacharias S (2006) Analysis of frequency and intensity of winter storm events in Europe on synoptic and regional scales from a multi-model perspective. Clim Res 31:59–74
Lunkheit F, Ponater M, Sausen R, M. Sogalla M, U. Ulbrich Windelband M (1996) Cyclonic activity in a warmer climate. Beitr Phys Atmos 69:393–407
Marsland SJ, Haak H, Jungclaus JH, Latif M, Röske F (2003) The Max-Planck-Institute global ocean/sea ice model with orthogonal curvilinear coordinates. Ocean Model 5:91–127
McCabe GJ, Clark MP, Serreze MC (2001) Trends in Northern Hemisphere surface cyclone frequency and intensity. J Clim 14:2763–2768
Murray RJ, Simmonds I (1991) A numerical scheme for tracking cyclone centres from digital data. Part I development and operation of the scheme. Aust Meteorol Mag 39:155–166
Nakamura H (1992) Midwinter suppression of barocline wave activity over the Pacific. J Atmos Sci 49:1629–1642
Nakićenović N, Alcamo J, Davis G, de Vries B, Fenhann J, Gaffin S, Gregory K, Grübler A, Jung TY, Kram T, La Rovere EL, Michaelis L, Mori S, Morita T, Pepper W, Pitcher H, Price L, Raihi K, Roehrl A, Rogner H-H, Sankovski A, Schlesinger M, Shukla P, Smith S, Swart R, van Rooijen S, Victor N, Dadi Z (2000) Emission scenarios. A special Report of Working Group III of the Intergovernmental Panel on Climate Change. Cambridge University Press, Cambridge, pp 599
Paciorek JC, Risbey JS, Ventura V, Rosen RD (2002) Multiple indices of Northern Hemisphere cyclonic activity, winters 1949–99. J Clim 15:1573–1590
Peixoto JP, Oort AH (1992) Physics of climate. American Institute of Physics, New York, pp 520
Pinto JG, Spangehl T, Ulbrich U, Speth P (2005) Sensitivities of a cyclone detection and tracking algorithm: individual tracks and climatology. Meteorol Z NF 14:823–838
Pinto JG, Spangehl T, Ulbrich U, Speth P (2006) Assessment of winter cyclone activity in a transient ECHAM4-OPYC3 GHG experiment. Meteorol Z NF 15:279–291
Räisänen J (2001) CO_2 induced climate change in CMIP2 experiments: quantifying of agreement and role of internal variability. J Clim 14:2088–2104
Roeckner E, Bäuml G, Bonaventura L, Brokopf R, Esch M, Giorgetta M, Hagemann, Kirchner I, Kornblueh L, Manzini E, Rhodin A, Schlese U, Schulzweida U, Tompkins A (2003) The atmospheric general circulation model ECHAM 5. PART I: model description. Max-Plank Institut Meteorol Rep 349, Hamburg
Roeckner E, Brokopf R, Esch M, Giorgetta M, Hagemann, Kornblueh L, Manzini E, Schlese U, Schulzweida U (2006) Sensitivity of simulated climate to horizontal and vertical resolution in the ECHAM5 atmosphere model. J Clim 19:3771–3791
Rogers J. C. 1990. Patterns of low-frequency monthly sea-level pressure variability (1899–1986) and associated wave cyclone frequencies. J Clim 3:1364–1379
Simmonds, I, Murray RJ, Leighton RM (1999) A refinement of cyclone tracking methods with data from FROST. Aust Meteorol Mag Spec Ed 35–49
Stephenson DB, Held IM (1993) GCM response of northern winter stationary waves and storm tracks to increasing amounts of carbone dioxide. J Clim 6:1859–1870
Tibaldi S, Molteni F (1990) On the operational predictability of blocking. Tellus 42A:343–365
Ulbrich U, Christoph M (1999) A shift of the NAO and increasing storm track activity over Europe due to anthropogenic greenhouse gas forcing. Clim Dyn 15:551–559
Wallace JM, Gutzler DS (1981) Teleconnections in the geopotential height field during the Northern Hemisphere winter season. Mon Weather Rev 109:784–812
Wallace JM, Lim G-H, Blackmon ML (1988) On the relationship between cyclone tracks, anticyclone tracks and baroclinic waveguides. J Atmos Sci 45:439–462
WASA (1998) Changing waves and storms in the Northeast Atlantic? Bull Am Meteorol Soc 79:741–760
Yin JH (2005) A consistent Poleward shift of the storm tracks in simulations of 21st century climate. Geophys Res Lett 32: L18701, doi: 10.1029/2005GL023684